Relativistic coupled-cluster-theory study for low-energy electron scattering with argon

Yongjun Cheng [1,*] Shi Liu [1] Song Bin Zhang [1] and Yong-Bo Tang [2,†]

[1] *School of Physics and Information Technology, Shaanxi Normal University, Xi'an 710119, People's Republic of China*

[2] *College of Engineering Physics, Shenzhen Technology University, Shenzhen 518118, People's Republic of China*

(Received 2 June 2020; accepted 14 July 2020; published 30 July 2020)

In this work, we carry out an comprehensive study for the electron scattering with atomic argon in the framework of relativistic box-variational method. The phase shifts first are extracted from relativistic coupled-cluster-theory calculations. Then the properties including total elastic, momentum transfer, viscosity cross sections, and differential cross sections are evaluated and compared with available experimental and theoretical data. The validity and accuracy of present method are verified by the good agreement with experimental values, especially for the differential cross sections at small angle forward and backward scattering where obvious discrepancies exist between experiments and theories. The predicted scattering length of $-1.39\ a_0$ for electron-argon system is only 2% larger in magnitude than the most recent experimental estimate. In addition, the role of electron correlation effect are also investigated in these properties.

DOI: 10.1103/PhysRevA.102.012824

I. INTRODUCTION

The low-energy elastic scattering of electrons on noble gases, in particularly on argon, is of particular interest in atomic and molecular physics for many decades [1]. One aspect is that reliable data for electron scattering from noble gases are of crucial importance in applications, such as electron-driven processes in phenomena of the earth and the planets, radiation chemistry, gaseous discharges, plasmas, and so on. On the other hand, many precise measurements are available in this energy region and they provide a fundamental test for theoretical methods. This is due to the fact that target preparation with light noble gases is straightforward, and the quality of existing data provided reference values for determining the instrumental response in experiments. Another reason is that the relativistic effect and target polarization play a dominant role in the low-energy scattering processes and this makes accurate theoretical treatment more challenging.

Although the treatment of correlation effect and relativistic nature has achieved a high level of accuracy in problems involving bound states, the situation is very different in the problems involving continuum states, such as the scattering problem. In the past few years, some new methods were proposed to convert the electron scattering problem to the problem of finding the solution of the Schrödinger equation including a series of discretized continuum states, or named as pseudocontinuum states. This is based on the fact that, when correct boundary conditions are applied, the pseudocontinuum states should be equivalent with true continuum states with same energies [2], since both wave functions are solutions of the same Schrödinger equation with same boundary conditions and same energies, although different normalization may be applied. Using these methods, the scattering parameters, such as the phase shifts and scattering length, are directly related to the discrete energies of pseudocontinuum states. Then the correlation and relativistic effect can be accurately accounted in exactly the same way as the bound state problems, and a high level of accuracy of scattering parameters could be expected by using the theoretical methods that has been proved to be capable of obtaining high precision discrete energy values.

The box-variational method [3,4] is such a very simple method converting the scattering problems to the discrete energies of pesudocontinuum states. In this approach, the system including the target and the incident electron is placed in an infinite wall cavity of radius R, chosen to be large enough that the wave function of scattered electron reach its asymptotic region. The discretized energies of the system in the cavity, E_n for a particular partial wave scattering, are obtained by solving the Schrödinger equation with the same boundary conditions, and then can be used to determine the phase shifts, δ, through a specific relation derived from the boundary conditions. The nonrelativistic box-variational method has been applied intermittently in a variety of contexts [5–9]. Recently, Cheng *et al.* developed a relativistic version of this method, and successfully used it to study low-energy electron scattering on atomic helium, neon, and krypton connected with an all-order single-double implementation of relativistic many-body perturbation theory [10]. The comparison with experimental values showed a good agreement.

Following that work [10], the present work carry out detailed studies of low-energy electron scattering with argon in the framework of relativistic box-variational method. Like as [10], B-splines basis set and the relativistic wave-function boundary conditions proposed by Johnson *et al.* [11] are used to expand the large, $P(r)$, and small, $Q(r)$, components of the Dirac wave function. Different with the work [10], an relativistic coupled-cluster (RCC) calculation starting from an no-pair Dirac-Coulomb-Breit Hamiltonian [12,13] is used to obtain discrete energies of the pseudocontinuum states of electron-argon system. Both linear and nonlinear terms within

*yjcphysics@163.com
†tangyongbo@sztu.edu.cn

the single- and double-excitations are included in correlation calculation. The nonlinear terms account for the contributions from many of the triple and quadruple determinant states, which is necessary for achieving high accurate energies. This approximation is termed as RCCSD-B-spline calculation.

In the present work, the scattering phase shifts were first extracted from the RCCSD-B-spline energies. Then we evaluated total elastic cross sections, momentum transfer cross sections, and viscosity cross sections at incident electron energies up to $k = 0.8$ a.u. ($E = 8.7$ eV), as well as the differential cross sections (DCS) at energies of 1, 3, 5, and 7.5 eV, and carried out a comprehensive comparison with available experimental and theoretical data. A good agreement in all these cross sections can be found especially in the DCS for small angle forward and backward scattering, where all the existing theoretical results significantly overestimated the experimental data. Our final predicted scattering length for electron-argon system is $-1.39\ a_0$, which is only 2% larger in magnitude than the most recent experimental estimate from Kurokawa *et al.* [14]. Atomic units will be used throughout, unless otherwise is explicitly stated.

II. FORMALISM

A. Box calculations and interpolation

The relativistic box-variational method is to extract phase shifts by applying the MIT/Notre Dame boundary conditions [11,15], $P(R) = Q(R)$, to the relativistic asymptotic form of the scattering wave functions with given energies. These energies are obtained by solving the Dirac equation for the system of target and incident electron in the same cavity with the same boundary conditions.

The radius of the cavity, R, is large so that the scattered electron at the boundary is described in asymptotic wavefunction showing oscillating behavior, and the true continuum states with certain energies could have nodes at the cavity radius and satisfy the boundary conditions, $P(R) = Q(R)$. Then the energies of these true continuum states could be predicted from energies of pseudocontinuum states with the same boundary conditions. A high level of accuracy can be expected as well as the discretized energies are produced very accurately. More energies can be obtained by continuously changing the radius of the cavity in a wide range. An interpolation procedure is also applied to obtain the phase shifts and cross sections at any energies.

We outline the essential features of the box calculation and interpolation procedure in this section, and more details can be found inRef. [10]. The relativistic asymptotic scattering wavefunctions are expressed as [16]

$$P(r) = krj_\ell(kr) - \tan(\delta)krn_\ell(kr) \tag{1}$$

and

$$Q(r) = \begin{cases} \dfrac{ck(krj_{\ell-1}(kr) - \tan(\delta)krn_{\ell-1}(kr))}{E + 2m_ec^2}, & \kappa > 0 \\ -\dfrac{ck(krj_{\ell+1}(kr) - \tan(\delta)krn_{\ell+1}(kr))}{E + 2m_ec^2}, & \kappa < 0 \end{cases}, \tag{2}$$

TABLE I. Interpolating functions, $w(\delta, k)$ for the phase shifts for each L value. The w_0 column gives the value of $w(\delta, k)$ for the final CCSD calculation in the $k = 0$ limit. The dipole polarizability for atomic Argon is $\alpha_d = 11.081$ a.u. [17].

L	$w(\delta, k)$	w_0	D	E
0	$-\dfrac{\tan(\delta) - E \times k^4 + \frac{\pi}{3}\alpha_d k^2}{k(1 + \frac{4}{3}\alpha_d k^2 \ln(k/D))}$	−1.39	0.045	−6.5
1	$\dfrac{\arctan(\frac{\pi}{15}\alpha_d k^2) - \delta}{k^3}$	11.8		
2	$\dfrac{\arctan(\frac{\pi}{105}\alpha_d k^2) - \delta}{k^3}$	0.96		
3	$\dfrac{\tan(\delta)}{k^2}$	0.064		

where j_ℓ and n_ℓ are spherical Bessel functions of the first and second kind. $\kappa > 0$ and $\kappa < 0$ represent the cases of $j = l - 1/2$ and $j = l + 1/2$, respectively.

The phase shifts then can be extracted by applying the boundary conditions to a pseudocontinuum state with energy E in a cavity of radius R as

$$\tan(\delta) = \begin{cases} \dfrac{-kcj_{\ell-1}(kR) - (E + 2m_ec^2)j_\ell(kR)}{-kcn_{l-1}(kR) - (E + 2m_ec^2)n_\ell(kR)}, & \kappa > 0 \\ \dfrac{-kcj_{\ell+1}(kR) + (E + 2m_ec^2)j_\ell(kR)}{-kcn_{\ell+1}(kR) + (E + 2m_ec^2)n_\ell(kR)}, & \kappa < 0 \end{cases}. \tag{3}$$

A further correction was also added to phase shift obtained at the cavity radius, R, to estimate the $r \to \infty$ phase shift. This correction was determined by integrating the Dirac equation, from $r = R$ to $r = 10R$ in a $-\alpha_d/(2r^4)$ potential field, where α_d is the static dipole polarizability [17]. The correction was found to be typically very small, only altering the phase shift in the fifth significant digit.

The present CCSD calculations are restricted to the states $\ell \leqslant 3$. Higher ℓ phase shifts are given by the modified effective range theory (MERT) [18–20],

$$\tan(\delta_\ell) = \frac{\pi\alpha_d k^2}{(2\ell - 1)(2\ell + 1)(2\ell + 3)}. \tag{4}$$

The error introduced by using MERT functions increases at larger energies [20]. However, the contribution from $\ell > 3$ states is expected to be very small up to a few tens electronvolts. In the present work, the largest percentage contribution from $\ell > 3$ states are found to occur at the minimum of the cross sections, being only about 1% for total cross sections and 0.6% for momentum transfer cross sections, thus the uncertainties introduced by using the MERT values should be negligible.

Application of box conditions to the CCSD calculation only gives the phase shifts at certain discrete energies in the continuum. In order to obtain the data at any energies, an interpolating procedure which has been previously utilized in our previous work [10] was adopted. The details of the functions used to create the phase shifts at any momentum of incident electron are tabulated in Table I. These functions are reliant on values of the dipole polarizability from Ref. [17] and the behavior of the interpolated phase shifts as a function

of energy was typically very smooth. The interpolation was done using natural cubic splines and the values of D and E are chosen manually to make $w(k,\delta)$ roughly constant at the smallest values of k.

B. The couple-cluster calculations

In the relativistic coupled cluster theory framework, the wave function of an atom with a valence orbital v is defined as

$$|\Psi_v\rangle = e^S|\Phi_v\rangle, \tag{5}$$

where the reference state $|\Phi_v\rangle$ is set as the lowest-order Dirac-Fock wave function. The cluster operator S is expressed as a sum of n-particle excitation S_n of the lowest-order wavefunction

$$S = \sum_{n=1}^{N} S_n = S_1 + S_2 + S_3 + \cdots, \tag{6}$$

where N is the number of electrons of a system. Only considering the linear single- and double- excitation approximation, the wave function is simplified as

$$|\Psi_v\rangle \approx (1 + S_1 + S_2)|\Phi_v\rangle. \tag{7}$$

This approximation is called LCCSD method, which is equal with the all-order method. If all non-linear terms of single- and double- excitation are also taken into account, the wave function is

$$\begin{aligned}|\Psi_v\rangle \approx \quad & \{1 + S_1 + S_2 + \frac{1}{2}(S_1^2 + S_2^2 + S_1S_2) \\ & + \frac{1}{6}(S_1^3 + 3S_1^2S_2) + \frac{1}{24}S_1^4\}|\Phi_v\rangle.\end{aligned} \tag{8}$$

This approximation is termed as CCSD method. The cluster excitations includes two classes from core and valence electrons, which are represented by $S^{(0,0)}$ and $S^{(0,1)}$, respectively, i.e.,

$$\begin{aligned}S &= S^{(0,0)} + S^{(0,1)} \\ &= S_1^{(0,0)} + S_2^{(0,0)} + S_1^{(0,1)} + S_2^{(0,1)}.\end{aligned} \tag{9}$$

In the language of second quantization, the cluster operator for core excitations is

$$\begin{aligned}S^{(0,0)} &= S_1^{(0,0)} + S_2^{(0,0)} \\ &= \sum_{ra} \{a_r^\dagger a_a\} s_a^r + \frac{1}{2}\sum_{rsab} \{a_r^\dagger a_s^\dagger a_a a_b\} s_{ab}^{rs},\end{aligned} \tag{10}$$

and the cluster operator for valence excitation is

$$\begin{aligned}S^{(0,1)} &= S_1^{(0,1)} + S_2^{(0,1)} \\ &= \sum_{r\neq v} \{a_r^\dagger a_v\} s_v^r + \sum_{rsa} \{a_r^\dagger a_s^\dagger a_v a_a\} s_{va}^{rs}.\end{aligned} \tag{11}$$

Above the alphabet a and b represent the core orbitals; r and s are designated as virtual orbitals; and v indicates valence states. $a^\dagger(a)$ are single-particle creation (annihilation) operator, and $s_{\cdots}^{\cdots}$ are cluster amplitudes. The cluster amplitudes and correlation energies are determined by solving the coupled equations derived from the generalized Bloch equations keeping only the connected terms.

$$Q[S_\ell^{(m,n)}, H_0]P = Q\{(V\Omega - \Omega H_{\rm eff})_\ell^{(m,n)}\}_{\rm conn} P, \tag{12}$$

$$H_{\rm eff} = P\big(V\Omega\big)_{\rm conn}^{(m,n)} P, \tag{13}$$

where P and Q are the usual projection operators which act on the model space and its orthogonal complement respectively, and $H_{\rm eff}$ represents the effective Hamiltonian.

In this work, we obtained the energies of pseudocontinuum states using the zero-order Dirac-Fock approximation based on the Dirac-Coulomb-Breit Hamiltonian (DCB), LCCSD, and CCSD methods, respectively. In Dirac-Fock calculation, we used 50 B-splines of order $k = 13$ to expand the large and small components of the radial wave functions. In coupled-cluster calculation, all core orbitals are set as active, the virtual orbitals with energies less than 1500 a.u. and partial waves with $\ell_{\rm max} < 6$ are included. The details of the method can be found in Refs. [12,13].

III. DATA ANALYSIS WITH DIFFERENT RADIUS

The determination of radius of the cavity is of vital importance in the box-variational calculation. Different discretized continuum states are obtained using different radius R of the B-spline basis. It has been stated in Ref. [2] that the pseudocontinuum states produced in a B-spline calculation with different radius can be interpreted as a representation of true continuum states with different normalization, and the pseudocontinuum with any energies can be obtained by properly adjusting the radius. Thus it is reasonable to perform calculations with different radius to examine the quality of discrete energies and also to obtain more energies to improve the accuracy level of the interpolation procedure.

In this paper, the discrete energies are obtained using the DCB, LCCSD and CCSD models and with $R = 40$, 56 and 80 a_0 for each model. The predicted energy rang is 0.04–0.40, 0.057–0.60, and 0.081–0.81 a.u. for $R = 80$, 56, and 40 a_0, respectively. Then we extracted the phase shifts from the energies and made an interpolation to get the phase shifts anywhere. The further long-range correction to the phase shift, made by integrating the $-\alpha_d/(2r^4)$ polarization potential outwards from $r = R$ to $10R$, was always less than 0.0001 rad with the correction being largest at the smallest energies. The final phase shifts obtained by using the energies with different radius in the interpolation are termed in the following discussions as DCB, LCCSD, and CCSD results, respectively. One should note that higher angular momentum B-spline basis should be included to represent the long-range behavior of the wave functions when the radius of cavity is enlarged. Since we used the same B-spline basis set in all the calculations, the quality of last two or three discrete energies would become worse with the increment of the radius.

Figure 1 plots $\tan\delta/k$ versus k, where k is the momentum of the incident electron, for s-wave to compare the CCSD phase shifts with different radius of the cavity. One can find noticeable irregularities in the energy dependence for R80 results when $k > 0.35$ a.u. and for R56 results when $k > 0.55$ a.u. Combining with the fact that the tail of R56 results show a better behavior than R80 results, the feature supported

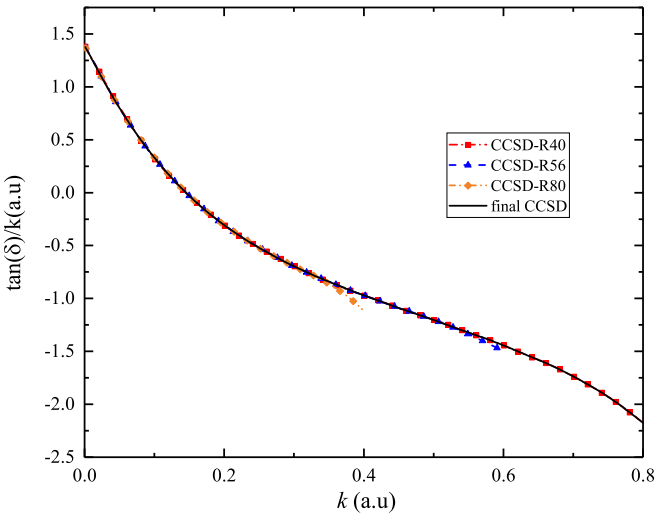

FIG. 1. The s-wave $\tan\delta/k$ vs k from the CCSD calculations with different radius for low-energy electron-argon scattering.

our prediction that higher energy levels would become worse when the radius becomes larger. So we only use the energies of R80 calculation when $k < 0.35$ a.u., R56 when $k < 0.55$ a.u., and all R40 results in the interpolation to obtain the final CCSD phase shifts. A quite similar phenomenon can also be found for DCB and LCCSD calculations with different radius of cavity that are not presented for the sake of clarity, thus a similar procedure is adopted to produce the final DCB and LCCSD results reported in this manuscript. Omitting the tails of the R56 and R80 calculations in Fig. 1, all results are almost indistinguishable from each other. This is an validation for the consistence of the present calculations with different radius. It is naturally to conclude that the discrete energy of any value between $0.04 - 0.8$ a.u. can be obtained by continuously changing the radius of cavity from 80 a.u. to 40 a.u., and the results should also agree with the final results presented here.

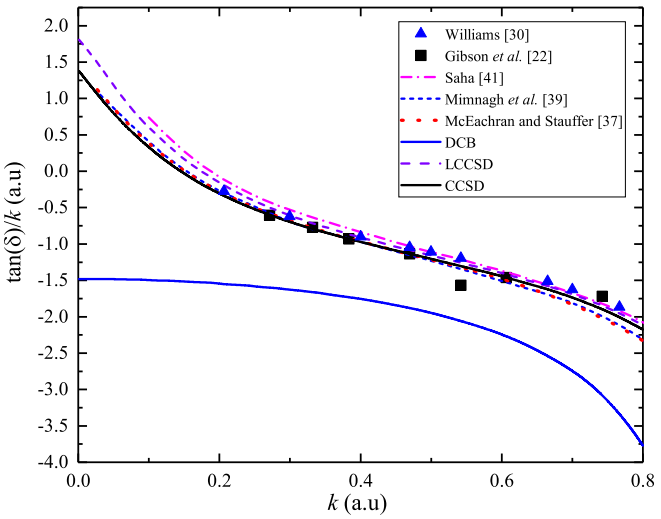

FIG. 2. The $\tan\delta/k$ vs k of s-wave for low-energy electron-argon scattering.

IV. COMPARISON WITH EXPERIMENTAL AND THEORETICAL DATA

The scattering of low-energy electron by argon has been the subject of extensive experimental and theoretical investigations. The crossed-beam technique is most frequently used to directly measure the differential cross sections (DCS). Then the integrated cross sections (ICS), including total cross sections, momentum transfer cross sections, and viscosity cross sections, can be obtained by integrating the DCS over the whole angular range. One important origin of uncertainties is the extrapolation procedure, which is always via phase-shift analysis or least-squares fitting with analytical functions, to get the cross sections at all angles. There have been a number of measurements performed using this technique and a series of phase shifts, DCS and ICS have been reported for electron-argon system [14,21–30]. Most of these measurements [21,22,24–26,29] are limited to relative measurements of cross sections, and the data needs to be scaled into absolute cross sections using the relative-flow technique or normalized to the existing benchmark data. There are also some direct measurement of the total cross sections [14,23,27,28] providing reliable upper bound of the cross-section data. The most recent measurement was performed by Kurokawa *et al.* [14] where a method for producing an electron beam at very low energy was developed and the grand total cross sections were reported from as low as 7 meV to 20 eV.

Swarm measurement is another widely used technique in electron-atom scattering. The distinguishing feature of this technique lies in the fact that they can provide absolute cross sections at low energies accounting for scattering through all angles. With some approximations to solve the Boltzmann equation, which are valid in low-energy electron scattering on noble gas atoms where only elastic scattering occurs, the total momentum transfer cross sections can be unfolded from the experimental data of the transport coefficients, such as the drift velocity and the diffusion coefficient. Then a phase shift analysis can be adopted on the swarm-derived cross sections to obtain the phase shifts and differential cross sections. The complicated unfolding procedure and the phase-shift analysis would introduce large uncertainties. Care must be taken in the procedure of theoretical analysis. The swarm-derived momentum transfer cross sections of low-energy electron-argon scattering have been reported by several groups [31–35]. The differential cross sections and total elastic cross sections are also reported by Haddad and O'Malley [34].

Obviously the phase shift analyzing, mostly based on the modified effective range theory (MERT) [18–20], is necessarily needed to obtain various cross sections and make direct comparisons between different measurements. It is also necessary in the extrapolation procedure from the existing experimental cross sections and theoretical phase shifts. The standard four parameter MERT (MERT4) expansion is valid to fit low-energy phase shift data and the uncertainty introduced is always less than 0.5% [20]. On the other hand, using MERT4 in the analyzing of experimental cross sections would introduce large uncertainties especially at energies below 0.5 eV where the correlation effect becomes dominant. So MERT5 or MERT6 (more higher order terms and adjustable parameters are added) is a more proper choice in these cases.

TABLE II. The CCSD phase shifts (in rad) for e^--Ar scattering. The first row for the δ_0 column gives the scattering length (in a_0).

k	δ_0	δ_1		δ_2			δ_3		
	s	$p_{\frac{1}{2}}$	$p_{\frac{3}{2}}$	$d_{\frac{3}{2}}$	$d_{\frac{5}{2}}$	MERT	$f_{\frac{5}{2}}$	$f_{\frac{7}{2}}$	MERT
0	−1.39								
0.05	0.03999	0.00434	0.00433	0.00069	0.00069	0.00083	0.00015	0.00015	0.00028
0.1	0.03308	0.01331	0.01317	0.00288	0.00288	0.00332	0.00073	0.00073	0.00111
0.2	−0.06107	0.02222	0.02132	0.01276	0.01277	0.01326	0.00358	0.00358	0.00442
0.3	−0.2058	−0.00303	−0.00531	0.03253	0.03257	0.02983	0.00856	0.00857	0.00995
0.4	−0.3704	−0.06543	−0.06926	0.06826	0.06841	0.05300	0.01594	0.01594	0.01768
0.5	−0.5420	−0.1547	−0.1601	0.1297	0.1301	0.08270	0.02599	0.02600	0.02762
0.6	−0.7138	−0.2587	−0.2654	0.2340	0.2342	0.11879	0.03928	0.03932	0.03976
0.7	−0.8824	−0.3692	−0.3771	0.3987	0.3998	0.16105	0.05647	0.05647	0.05410
0.8	−1.049	−0.4815	−0.4903	0.6401	0.6412	0.20909	0.07691	0.07690	0.07061

On the theoretical side, the phase shifts, differential and integrated cross sections for low-energy electron scattering on argon were reported by complex optical potential (COP) calculations of McEachran and Stauffer [36–38] and Mimnagh *et al.* [39], the MCHF calculations of Saha [40,41], the B-spline R-matrix (BSR) calculation of Zatsarinny *et al.* [42], and a number earlier calculations [43–48]. Note that the BSR differential and integrated cross section can be found in the LXcat database [49]. There are also two comprehensive studies for *e*-Ar scattering in a large energy region from Adibzadeh and Theodosiou [50] and Haque *et al.* [51]. However, the agreement between theory and experiments is still not satisfactory especially in the case of differential cross sections. For the sake of clarity, at all the cases presented in this paper, we show only a few of the calculated cross sections which demonstrate the best accord with experiment.

A. phase shifts and scattering length

The results of $\tan\delta/k$ versus k for s-wave of final DCB, LCCSD and CCSD calculations are compared with available theoretical [37,39,40] and experimental data [22,29,30] in Fig. 2. The importance of the correlation effect can be found in the significantly lower values of DCB results. The DCB value is always negative because the polarization effect is neglected and then the interaction between the incident electron and the target is repulsive. In the LCCSD calculations, the phase shifts is positive at $k < 0.175$ a.u. since the polarization effect leads to the projectile-target interaction being attractive at very low energies. The phase shifts in CCSD calculations, in which the nonlinear terms are incorporated, is positive when $k < 0.146$ a.u. indicating a less attractive projectile-target interaction. The obviously lower values of the CCSD calculation comparing with the LCCSD results reveals the importance of including nonlinear terms in the coupled-cluster calculation at very low energies. The LCCSD and the MCHF results of Saha [40] tend to be larger below 0.2 a.u., while the COP calculations [37,39] are slightly lower above 0.6 a.u. The present CCSD values are in a close agreement with the experimental data of Gibson *et al.* [22] and Williams [30]. The one exception occurs at $k = 0.54$ a.u. where the measurement of Gibson *et al.* [22] appears to have an irregularity. The uncertainties of the measurement of Williams [30] are reported to be from 3% to 5% and the corresponding error bars are not displayed in the figure.

The CCSD phase shifts for the individual partial waves, along with the integrated cross sections, are tabulated in Tables II and III, respectively. The s-wave and p-wave phase shifts go through zero for momentum between 0.1 and 0.2 a.u., and 0.2 and 0.3 a.u., respectively. This contributes to the depth of the well-known Ramsauer-Townsend (RT) minimum that we can find in the cross sections in the following parts. The MERT values for the d-wave and f-wave are also presented for comparison. The CCSD phase shifts at the lowest energies for the d-wave and f-wave did not converge to the MERT formula as expected. Although these partial waves only contribute to the cross sections by less than 4% when $k \leqslant 0.1$ a.u., this do indicate the incompleteness of the description for the electron-atom polarization in the present methodology.

Scattering lengths, which is directly related to the cross sections at zero limit, are listed in Table IV comparing with previous reported studies. As discussed above, the DCB value of scattering length is positive because the polarization effect is excluded and the interaction between the incident electron and the target is repulsive. The negative values of scattering lengths for LCCSD and CCSD calculations show that the polarization leads to this effective interaction being attractive. A smaller value of -1.39 a_0 is predicted in our CCSD calculation and this is due to a less attractive interaction with

TABLE III. The CCSD total elastic cross sections $\sigma_{\rm T}$, momentum transfer cross sections $\sigma_{\rm MT}$, and viscosity cross sections $\sigma_{\rm V}$ (in πa_0^2) for e^--Ar scattering.

k	$\sigma_{\rm T}$	$\sigma_{\rm MT}$	$\sigma_{\rm V}$
0	7.7284	7.7284	
0.05	2.734	2.126	1.682
0.1	0.6501	0.2343	0.3222
0.2	0.6126	0.7300	0.4239
0.3	2.111	1.958	1.725
0.4	4.277	3.358	3.384
0.5	6.897	5.359	5.172
0.6	10.18	8.440	6.972
0.7	14.57	12.72	8.627
0.8	20.35	17.40	9.816

TABLE IV. The scattering length (in a_0) for e^--Ar scattering. The BSR value is derived from its zero-energy momentum transfer cross sections in the LXcat database [49].

	$A_{\rm scat}$ (a_0)
theory	
DCB	1.48
LCCSD	−1.82
CCSD	−1.39
Saha [41]	−1.486
McEachran and Stauffer [37]	−1.441
Mimnagh *et al.* [39]	−1.386
Bell *et al.* [47]	−1.68
BSR [49]	−1.449
experiment	
Haddad and O'Malley [34]	−1.488
Ferch and Raith [28]	−1.449
Weyhreter *et al.* [25]	−1.593
Buckman and Mitroy [20]	−1.442
Petrovic *et al.* [52]	−1.459
Kurokawa *et al.* [14]	−1.365(5)

the inclusion of nonlinear terms. The 30% differences between LCCSD and CCSD scattering lengths indicate that the nonlinear terms have a big impact on the scattering lengths.

Most of the experimental predictions for scattering lengths lie in the range of -1.44 a_0 and -1.60 a_0, except the most recent measurement from Kurokawa *et al.* [14]. However, scattering lengths are estimated by MERT analysis of cross sections or phase shifts at finite energies, and these are obtained from the measurements mostly restricted at a relatively higher energy range ($\geqslant$50 meV), thus it may have uncertainty in extrapolating the cross-section curve down to zero energy by the MERT fit. Especially for swarm experiments, deriving the momentum transfer cross sections from the macroscopic experimental results includes a complicated and cumbersome unfolding procedure that is another important origin of uncertainty. Another important factor is the functional form of the MERT expressions used to extract the scattering length. As we discussed above, using MERT4 in analyzing of experimental cross sections would introduce large uncertainties especially at energies below 0.5 eV. The experiment of Kurokawa *et al.* [14] is a single-collision measurement starting from as low as 7 meV and an extended version of MERT6 formula was used to minimize the uncertainty. They reported a value of scattering length of $-1.365[5]$ a_0. On the theoretical side, the value of Bell *et al.* [47] is -1.65 a_0 being larger than all other results. The MCHF scattering length of -1.486 a_0 shows excellent agreement with the experimental value from [34]. The nonrelativistic COP calculation [39] included the dynamic distortion effects and predicted a value of -1.386 a_0, whereas their later relativistic calculation in Ref. [37] gives a scattering length of -1.441 a_0. Their calculations also indicate that relativistic effects are significant at energies below 5 eV, giving rise to $p_{1/2}$ and $p_{3/2}$ phase shifts which differ by 20% at 1 eV and 3% at 3 eV. The BSR value of -1.449 a_0 is derived from its zero-energy momentum transfer cross sections, 7.387200×10^{-20} m^2, from the LXcat database [49]. Both the BSR and relativistic COP scattering lengths agree well with experimental predictions from [20,28]. The present CCSD scattering length of -1.39 a_0 differs with the value of Ref. [14] only by less than 2%. More measurement at much lower energies are needed to precisely determine the scattering length for electron-argon scattering.

B. Differential cross sections

The differential cross section $\sigma_{e\ell}(\theta)$ is calculated as

$$\sigma_{e\ell}(\theta) = |f(\theta)|^2 + |g(\theta)|^2, \tag{14}$$

where $f(\theta)$ and $g(\theta)$ are the direct and spin-flip scattering amplitudes, respectively. The relativistic amplitudes and the T-matrix element are calculated as

$$f(\theta) = \frac{1}{k}\sum_{\ell=0}^{\infty}((\ell+1)T_\ell^+(k) + \ell T_\ell^-(k))P_\ell(\cos\theta), \tag{15}$$

$$g(\theta) = \frac{1}{k}\sum_{\ell=0}^{\infty}(T_\ell^-(k) - T_\ell^+(k))P_\ell^1(\cos\theta), \tag{16}$$

$$T_\ell^\pm(k) = e^{i\delta_\ell^\pm(k)}\sin(\delta_\ell^\pm(k)). \tag{17}$$

In these equations, δ_ℓ^+ refers to the phase shift with $j = \ell + \frac{1}{2}$ and δ_ℓ^- refers to the phase shift with $j = \ell - \frac{1}{2}$.

Comparing with the integrated cross sections presented in the following part, the differential cross section is a more strict test for different theoretical method since the DCS is much more sensitive to the description of the relativistic nature and target polarization effect of the electron-target system. Actually obviously discrepancies can be found between the existing theoretical and experimental data at the DCS of low-energy forward and backward electron-argon scattering and the differences could be as large as 20% as we can find in the following figures.

The DCB, LCCSD and CCSD calculations of differential cross sections (DCS) for incident electron energies of 1, 3, 5, and 7.5 eV are presented in Fig. 3 to verify the effect of different treatment for the polarization. Note that the *s*-wave contribution to the DCS is the same at all angles and the minima are mainly determined from the *p*-wave and *d*-wave. At 1 eV, the fact that DCB cross sections are approximately one order larger at all angles indicates that the correlation effect plays a dominant role in the scattering process at such a low energy. The LCCSD and CCSD calculations exhibited obvious discrepancies at small angles. As energy increases, the DCB and LCCSD calculations behave better especially at the angles larger than 90°. The DCB cross sections at 7.5 eV are only slightly larger above 140° and below 40°. The difference between LCCSD and CCSD cross sections is almost negligible at 5 and 7.5 eV above 60°. However, the LCCSD results still always have a marginally deeper minimum at a slightly larger angle. These features conclude that the target polarization is less important above 7.5 eV and a more complete description of the polarization effect is essential to obtain more accurate differential cross sections below 5 eV especially below 60° and around the minimum.

The present CCSD DCS are compared with the most recent experimental and theoretical data in Figs. 4–7. At 1.0 eV, the measurements of Gibson *et al.* [22], Weyhreter *et al.* [25] and Haddad and O'Malley [34], and the COP calculations of

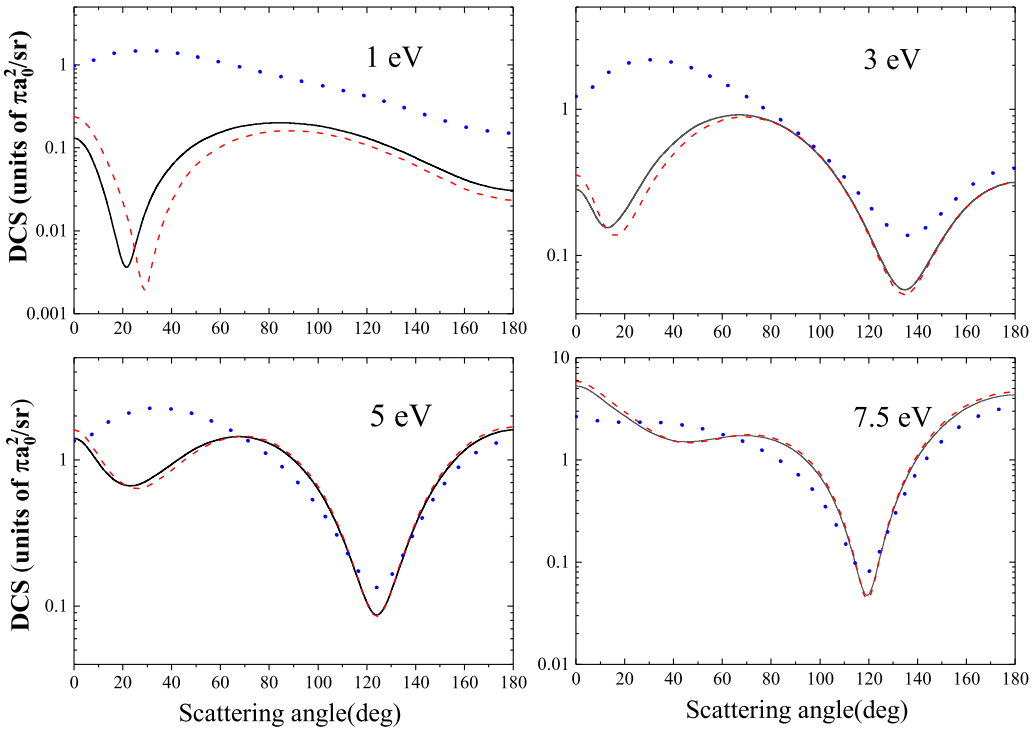

FIG. 3. The present differential cross sections (in πa_0^2) for low-energy electron-argon scattering. CCSD cross sections (solid), LCCSD cross sections (dashed line), and DCB cross sections (dotted line).

McEachran and Stauffer [37] are displayed for comparison. Note that the BSR cross sections at 0.952 eV [49] are also shown in the figure. This is reasonable since we have checked that our CCSD results at 0.952 eV are indistinguishable from that at 1 eV. Weyhreter *et al.* [25] stated their uncertainties to be from 0.1% to 1.2% which is too small to be shown in the figure. Gibson *et al.* [22] gives the uncertainties of typically around 10% at most of angles, while the uncertainty is as large as almost 100% at their smallest angle 30° due to the very small cross sections. The measurements of Gibson *et al.* [22] and Weyhreter *et al.* [25] shows excellent agreement, but both of them did not give any data below 20° and the position of minimum cannot be identified. Haddad and O'Malley [34] reported their cross section from 3° but their results are significantly larger than other data at angles above 30°. Our CCSD cross sections predicted a minimum at 20°, which is close to the data of Haddad and O'Malley [34], and agree well with their cross sections below 20°. The BSR and COP cross sections agree well with each other between 10° and 30°, and both of them predicted a minimum at 25°. At angles larger than 60°, all the theoretical cross sections show excellent agreement with the experimental data of Gibson *et al.* [22] and Weyhreter *et al.* [25]. Between 30° and 60°, the CCSD and BSR cross sections are slightly larger but all theoretical data are lying within the uncertainties of these two experiments.

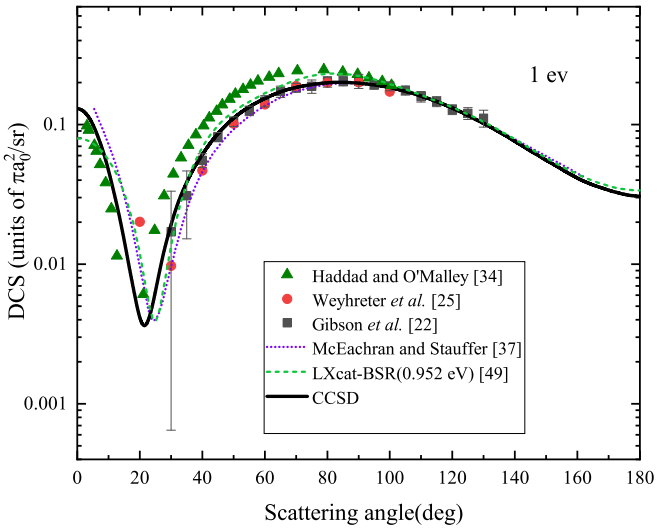

FIG. 4. The differential cross section (in πa_0^2) with the incident electron energy 1 eV for low-energy electron-argon scattering.

In Fig. 5, our CCSD DCS at 3 eV are compared with the measurements of Gibson *et al.* [22], Furst *et al.* [24], and Srivastava *et al.* [29], and the COP calculations of McEachran and Stauffer [37], the optical potential model (OPM) calculation of Haque *et al.* [51], and the BSR cross sections at 2.993 eV [49]. Most of these measurements, as well as the measurements displayed in Figs. 6 and 7, are reported with uncertainties from 6% to 15%. Srivastava *et al.* [29] stated their uncertainties to be 20% at all the angles. A distinct feature of Fig. 5 is the appearance of the second minimum which is much smaller than the first minimum. Unfortunately although the experimental data are all lying within the uncertainties of each other, they are all restricted in the angle range between 20° and 130° and can not give any information about the position of both minima. All the theoretical calculations revealed the existence of two minima but predicted slightly different magnitudes and positions. With the outlier of the OPM cross

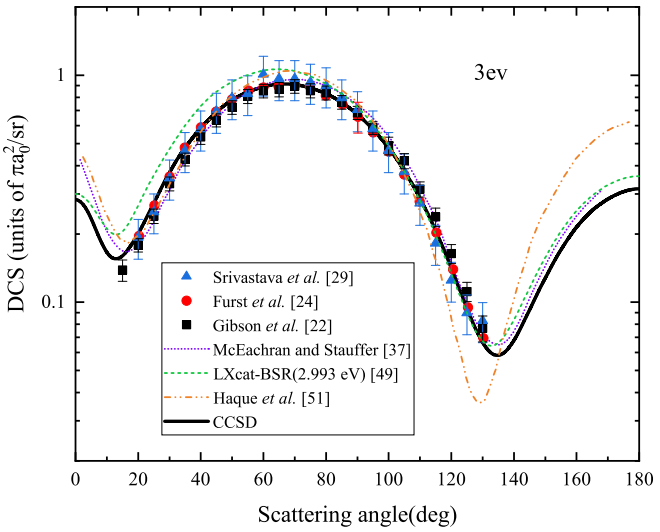

FIG. 5. The differential cross section (in πa_0^2) with the incident electron energy 3 eV for low-energy electron-argon scattering.

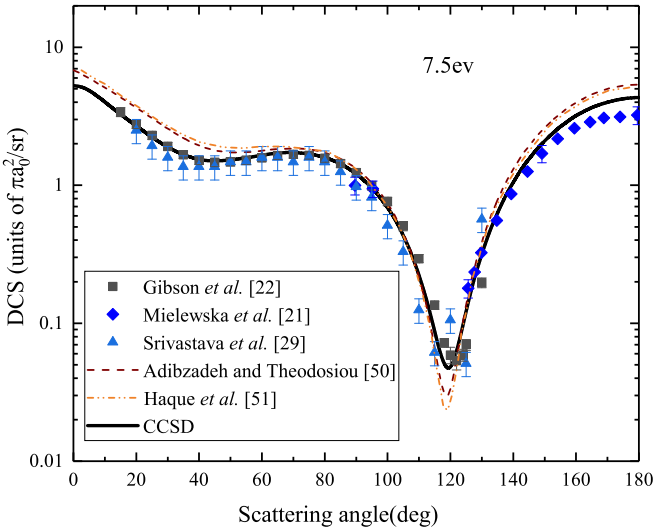

FIG. 7. The differential cross section (in πa_0^2) with the incident electron energy 7.5 eV for low-energy electron-argon scattering.

sections [51], most of the theoretical data agree well with the experimental measurements in the angular range between two minima but shows obvious discrepancies outside this range. The BSR DCS are above all other cross sections between 15° and 60° while the OPM cross sections are significantly larger above 140°. The present CCSD DCS tend to be the lowest one below our first minimum around 15° and above the second minimum at 135°. This phenomenon can also be found in the DCS at 5 and 7.5 eV where the CCSD calculation also gives the lowest cross sections. More detailed measurements at this angular range are needed to verify different theoretical models.

The CCSD DCS at 5 eV are plotted in Fig. 6 and compared with the measurements of Mielewska *et al.* [21], Gibson *et al.* [22], Furst *et al.* [24], and Srivastava *et al.* [29], and the calculations of McEachran and Stauffer [37], Adibzadeh and Theodosiou [50], and Haque *et al.* [51]. The measurements

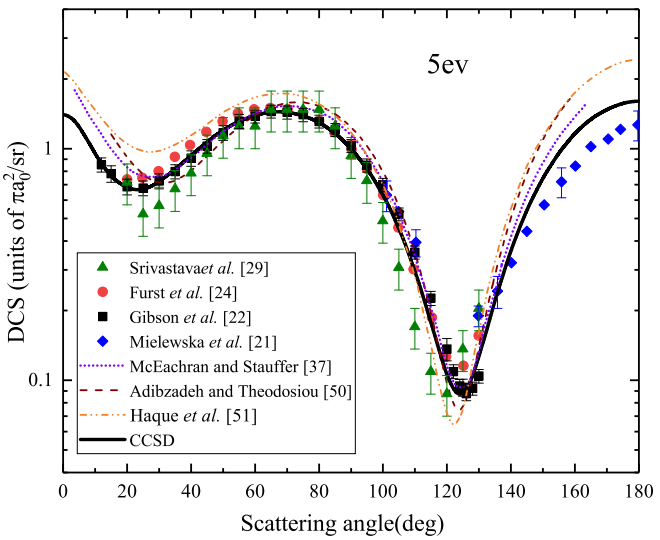

FIG. 6. The differential cross section (in πa_0^2) with the incident electron energy 5 eV for low-energy electron-argon scattering.

were in a larger angular range and the positions of two minima are revealed at around 25° and 125° that are consistent with present CCSD calculation. The situation is similar with the case at 3 eV. With the exception of the DCS from Haque *et al.* [51], the agreement level between the two minima are excellent among the theoretical and experimental data, while our CCSD cross sections are the lowest theoretical data outside this angular range where all the experimental data also produced significantly lower cross sections. Although obviously larger than the data of Mielewska *et al.* [21] above 140°, our CCSD cross sections behave better than other calculations and tend to be the only theoretical data that shows excellent agreement with the measurements of Gibson *et al.* [22] and Furst *et al.* [24] at the angles below 30°.

A very much similar situation can be found in the DCS at 7.5 eV in Fig. 7 where our CCSD DCS are compared with the measurements of Mielewska *et al.* [21], Gibson *et al.* [22], and Srivastava *et al.* [29], and the calculations of Adibzadeh and Theodosiou [50] and Haque *et al.* [51]. The calculations from Adibzadeh and Theodosiou [50] and Haque *et al.* [51] in which different model potentials are used to study the electron-argon scattering in a very large energy range both yield obviously larger cross sections below 60° and above 140°, and their calculations also predicted a much deeper second minimum. Our CCSD cross sections are once again the only theoretical data that shows excellent agreement with the experimental data below 60° and shows much better agreement than other calculations above 140°. As a further check, we also compared our CCSD DCS at 4.898 and 7.619 eV with the BSR DCS [49]. The comparisons are not presented here for simplicity. Both calculations yield the same positions of the two minima at both energies. The BSR DCS are significantly larger than CCSD DCS below 80° at 4.898 eV, while they show excellent agreement above 80° at 4.898 eV and at the whole angular range at 7.619 eV.

By checking the DCS in these energies, one can conclude that most of the theoretical data including our CCSD results are in a close agreement with the experimental data in the

central range (30°–140°), while all the previous theoretical calculations significantly overestimated the experimental cross sections outside this angular range. This discrepancy is probably due to the incomplete description of the correlation effect and the relativistic nature. By taking both linear and nonlinear terms into account in the single- and double-excitation coupled cluster calculations, our CCSD cross sections resolved the discrepancy below 30° and shows excellent agreement with experiments. Furthermore, the CCSD DCS also shows a better agreement with experiments above 140°. Generally the present CCSD differential cross sections shows by far the best agreement with existing experimental measurements.

C. Integrated cross sections

Various accurate integrated cross sections for low-energy electron scattering are of crucial importance for determining the atomic and molecular structure and studying electron transport in matter, and are also needed in many applications.

The total cross section σ_T is one of the most reliable quantities to characterize the scattering process since it can be determined without any normalization procedure. Therefore it may serve as a standard value (an upper limit) for the normalization of data for individual scattering process and/or as a test of theoretical models. The higher-order cross sections σ_r, usually referred to as momentum transfer cross sections σ_{MT} when $r = 1$ and as viscosity cross sections σ_V when $r = 2$, are also of particular importance in various domains of electron kinetic and transport theories. For example, both cross sections are necessary in solving the multiterm Boltzmann equation to establish the form of the electron steady-state distribution function for a weakly ionized plasma placed in an external dc electric field. These cross sections are usually defined as

$$\sigma_T = 2\pi \int_0^\pi \sigma_{e\ell}(\theta) \sin\theta d\theta, \tag{18}$$

$$\sigma_r = 2\pi \int_0^\pi \sigma_{e\ell}(\theta)(1 - \cos^r\theta) \sin\theta d\theta. \tag{19}$$

Then we can obtain the cross sections as

$$\sigma_T = \frac{4\pi}{k^2} \sum_{\ell=0}^{\infty} \left((\ell+1)\sin^2(\delta_\ell^+) + \ell \sin^2(\delta_\ell^-)\right), \tag{20}$$

$$\sigma_{MT} = \frac{4\pi}{k^2} \sum_{\ell=0}^{\infty} \left(\frac{(\ell+1)(\ell+2)}{(2\ell+3)} \sin^2(\delta_\ell^+ - \delta_{\ell+1}^+) + \frac{\ell(\ell+1)}{(2\ell+1)} \sin^2(\delta_\ell^- - \delta_{\ell+1}^-) + \frac{(\ell+1)}{(2\ell+1)(2\ell+3)} \sin^2(\delta_\ell^+ - \delta_{\ell+1}^-) \right), \tag{21}$$

$$\sigma_V = \frac{4\pi}{k^2} \sum_{\ell=0}^{\infty} \left(\frac{2\ell(\ell+1)}{(2\ell-1)(2\ell+1)(2\ell+3)} \sin^2(\delta_\ell^+ - \delta_\ell^-) + \frac{\ell(\ell+1)(\ell+2)}{(2\ell+1)(2\ell+3)} \sin^2(\delta_\ell^- - \delta_{\ell+2}^-) + \frac{(\ell+1)(\ell+2)(\ell+3)}{(2\ell+3)(2\ell+5)} \sin^2(\delta_\ell^+ - \delta_{\ell+2}^+) + \frac{2(\ell+1)(\ell+2)}{(2\ell+1)(2\ell+3)(2\ell+5)} \sin^2(\delta_\ell^+ - \delta_{\ell+2}^-) \right). \tag{22}$$

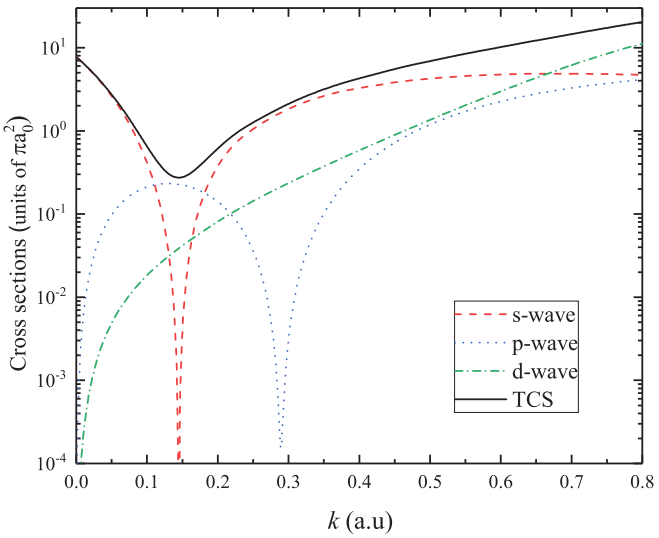

FIG. 8. The individual *s*-, *p*-, and *d*-wave contribution to the total elastic cross sections (TCS).

Our cross sections from DCB, LCCSD, and CCSD calculations are presented and compared with available experimental and theoretical data in Figs. 9–11, respectively. A dominant feature of the integrated cross sections for electron-rare gas scattering is the existence of Ramsauer-Townsend (RT) minimum. The individual contributions from *s*-, *p*-, and *d*-waves to the total cross sections are displayed in Fig. 8 to explain this. The *s*-wave cross sections decrease to zero rapidly and then rise as the energy increases. The minimum occurs when the *s*-wave contribution is almost negligible and the contributions from other partial waves are still small. The prediction of RT minimum is a critical test for experiment and theory.

There have been a number of experimental and theoretical total elastic and momentum transfer cross sections reported for electron-argon system. To avoid cluttering the graph, the presentation of data from other sources has been selective.

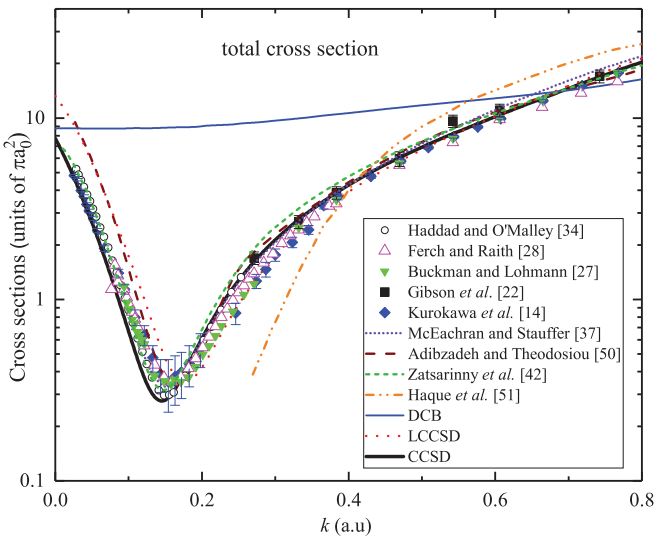

FIG. 9. The elastic cross section (in πa_0^2) as a function of momentum (in a.u.) for low-energy electron-argon scattering.

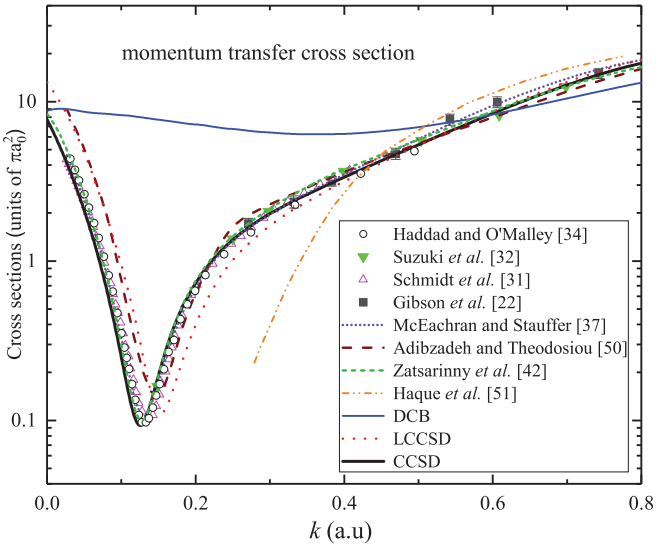

FIG. 10. The momentum transfer cross section (in πa_0^2) as a function of momentum (in a.u.) for low-energy electron-Ar scattering.

Only some recent measurements covering the position of RT minimum and the theoretical calculations showing the best accordance with experimental data are depicted in Figs. 9 and 10. The displayed theoretical cross sections are the relativistic COP calculation of McEachran and Stauffer [37], the BSR calculation of Zatsarinny *et al.* [42], the model potential calculation of Adibzadeh and Theodosiou [50], and the most recent OPM calculation of Haque *et al.* [51]. Note that the OPM calculations are performed in the energy range from 1 eV to 0.5 GeV. Their cross sections behave well at middle and high energies but are significantly different from all other data sets in the energy region discussed in this work.

In Fig. 9, the beam experiments of Kurokawa *et al.* [14], Gibson *et al.* [22], Buckman and Lohmann [27], Ferch and Raith [28], and the swarm derived results of Haddad and

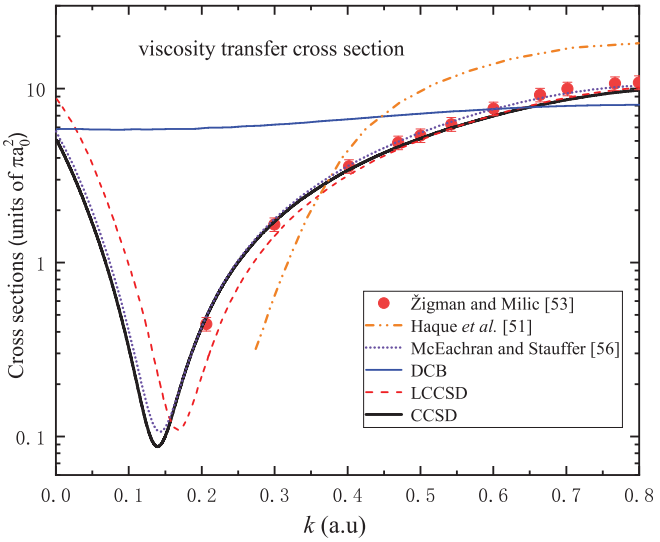

FIG. 11. The viscosity cross section (in πa_0^2) as a function of momentum (in a.u.) for low-energy electron-Ar scattering.

O'Malley [34] are presented for comparison. The measurement of Kurokawa *et al.* [14] has a relatively larger uncertainties, which range from 10% to 30%, around the position of RT minimum. The uncertainties decrease to only 1% or 2% at the energies far from the minimum, then one cannot find the error bar in the figure. Gibson *et al.* [22] reported their total cross sections, as well as momentum transfer cross sections in Fig. 10, at the energies above the RT minimum with an uncertainty of typically from 7% to 9%. The reported uncertainties varies from 3% to 6% for the measurement of Buckman and Lohmann [27], in which the uncertainties decrease as the energy increases, and from 1% to 3% for Ferch and Raith [28] where the largest uncertainty occurs around the RT minimum. The error bars of both two sets of data are so small that they are not displayed in the figure for the sake of simplicity.

The cross sections show a steep increase as energies decrease below the RT minimum. Once again the absence of target polarization in DCB model leads to quite different cross sections and the difference tends to be smaller as the energy increases. The inclusion of nonlinear terms in the CCSD calculation gives the RT minimum at $k = 0.145$ a.u. ($E = 0.286$ eV) being slightly smaller than the LCCSD value of $k = 0.177$ a.u. ($E = 0.426$ eV). The LCCSD cross sections merge into the CCSD results above 0.5 a.u.. Similar phenomenon for DCB and LCCSD results can also be found in Figs. 10 and 11. There is a tendency for difference between theory and experiment to vanish at energies above the RT minimum with only one exception of Haque *et al.* [51]. This cancellation of differences was also apparent in comparisons of momentum transfer cross sections in Fig. 10. At the energies below the RT minimum, the results of Adibzadeh and Theodosiou [50] tend to obviously overestimate the cross sections, whereas the CCSD, BSR [42], and relativistic COP [37] cross sections are in a close agreement with experimental data. The most obvious discrepancy occurs at the position of the RT minimum. Our CCSD value of 0.286 eV is close to 0.298 eV for both the measurements of Haddad and O'Malley and the BSR calculations, while other theoretical and experimental RT minimum are at 0.323 eV for Ref. [14], 0.340 eV for Ref. [27], 0.345 eV for Ref. [28], 0.310 eV for Ref. [37], and 0.400 eV for Ref. [50], respectively. The theoretical prediction of RT minimum is very sensitive to the fine details of the projectile-target interaction, however, the CCSD, BSR, and COP predictions exhibit a reasonable agreement. The experimental values of RT minimum differ with each other obviously and the measurements all have large uncertainties. More measurements are needed to precisely determine the location of the RT minimum.

The momentum transfer cross sections are compared with the swarm derived results of Schmidt *et al.* [31], Suzuki *et al.* [32], and Haddad and O'Malley [34], and the phase shift derived results of Gibson *et al.* [22] in Fig. 10. A similar situation with the case of total cross section can be found. The CCSD RT minimum is at $k = 0.125$ a.u. ($E = 0.213$ eV) while it is at $k = 0.153$ a.u. ($E = 0.318$ eV) in LCCSD cross sections. The calculation of Adibzadeh and Theodosiou [50] once again tends to overestimate the cross section at the energies below the RT minimum, the OPM calculation of Haque *et al.* [51] is an outlier, while the CCSD, BSR [42], and COP [37] cross

sections are all in a close agreement with experimental data. The CCSD RT minimum is close to 0.219 eV for both the measurements of Haddad and O'Malley and the BSR calculations, while other theoretical and experimental RT minimum are at 0.244 eV for Ref. [32], 0.230 eV for Ref. [37], and 0.400 eV for Ref. [50], respectively.

The viscosity cross sections plotted in Fig. 11 are also of particular interest in many fields. For instance, it will be encountered in the kinetic theory of viscous effects and it is also necessary in the solutions of the Boltzmann Equation going beyond the two-term approximation [53,54]. However, this fact seems to have lacked adequate emphasis in the literature. To the best of our knowledge, the viscosity cross sections for electron-argon system are only reported from beam experiments by Panajotovic *et al.* [55] above 10 eV, and from a MERT analysis by Zigman and Milic [53] above 0.13 eV using phase shifts from the measurements of Williams [30], respectively. A very sophisticated fitting procedure is developed and the viscosity cross sections are reported in a relativistic COP calculation from McEachran and Stauffer [56]. More recently, the OPM calculation of Haque *et al.* [51] also reported the viscosity cross sections from 1 eV to 0.5 GeV. However, the low-energy OPM cross sections are significantly different from other sets of data. A good agreement can be found between the CCSD and COP cross sections [56], and both calculations lie within the uncertainties of the cross sections obtained from the phase shifts of Williams [30], where the uncertainties are given to be approximately 9%. However, the position of RT minimum cannot be determined from the experimental data. Once again an indication of the impact of correlation effect and the nonlinear terms can be gained from the comparison among our DCB, LCCSD and CCSD cross sections that are very similar with the situation in total elastic and momentum transfer cross sections. The CCSD RT minimum is at $k = 0.14$ a.u. ($E = 0.267$ eV) being slightly smaller than the LCCSD results of $k = 0.168$ a.u. ($E = 0.384$ eV).

V. PERSPECTIVES AND CONCLUSIONS

In the present manuscript, the idea of box-variational method are applied to the description of low-energy electron-argon scattering by combining relativistic coupled-cluster method considering all nonlinear and linear single-double approximation. The phase shifts are extracted and then used to obtain a further set of differential cross sections, total elastic, momentum transfer, and viscosity cross sections. The impact of the correlation effect at different energy regions is revealed by the comparison among DCB, LCCSD, and CCSD calculations in various cross sections. The cross sections are proved to be very sensitive to the description of correlation effect particularly at the energies below 5 eV.

The validity and accuracy of our method are verified by the good agreement between the present CCSD data with experiments. The CCSD DCS shows excellent agreement with most of existing experimental data in both forward and central angular regions, especially at the forward scattering where the previous theoretical DCS significantly overestimated experimental data. In terms of the integrated cross sections, our CCSD total elastic, momentum transfer, and viscosity cross sections also exhibit a good agreement with the experiments and the relativistic dynamic distortion calculations of McEachran and Stauffer [37,56] and the BSR calculations of Zatsarinny *et al.* [42] with the only exception being slight difference in the position of the Ramsauer-Townsend minimum. The scattering length is an important parameter characterizing the incident electron-target interaction at very low energies. Our predicted scattering length differs by less than 2% with the value derived from the analysis of the most recent beam experiments [14].

Examination of the DCS at different energies reveals some interesting features. Although the present CCSD DCS has exhibited by far the best agreement with experiments, our cross sections still obviously overestimated the experimental data in the backward scattering. Another worth noting point is at the phase shifts of higher ℓ partial waves. At the lowest energies for the higher ℓ partial waves, one expects calculated phase shifts to converge to the MERT formula. However, this does not occur. The present CCSD d-wave and f-wave phase shifts are slightly smaller than the MERT phase shifts. These features do not have much impact on the cross sections. But they do indicate that a theoretical methodology that includes nonlinear terms of single and double excitations does not capture 100% of the electron-atom polarization interaction. A proper treatment of triple and higher order excitations is needed.

The emphasis of the most recent electron scattering researches has been focused on developing theories that do a reasonable job of modeling excitation and ionization over a large energy range rather than purely elastic scattering. However, the very low-energy scattering is the most sensitive to the fine details of the electron-atom interaction and it is a critical test for theories. The application of the method to more complex rare gas systems where spin-exchange effect is more obvious would be straightforward. Modification of the method aiming the application to energy regions where inelastic events are possible is also developing. The present study also paved a way to apply the box-variational method to low-energy electron-molecule scattering. Obtaining accurate data for low-energy electron-molecule scattering is a very challenging task, however, such information are indeed needed for electron-impact chemistry [57]. The box-variational method bypasses many complications in existing scattering calculations, and provides a relatively simple way to extract the scattering information from accurate energies of discretized continuum states of electron-molecule system which can be solved using existing methods.

ACKNOWLEDGMENTS

We gratefully acknowledge the support from the National Natural Science Foundation of China Grants No. 11974230, No. 11934004 and No. 11504094, and Post-doctoral research project of SZTU No. 202028555301011. We are grateful to Prof. T.-Y. Shi for the valuable discussions.

[1] A. Zecca, G. P. Karwasz, and R. S. Brusa, Riv. Nuovo Cimento **19**, 1 (1996).
[2] H. Bachau, E. Cormier, P. Decleva, J. E. Hansen, and F. Martín, Rep. Prog. Phys. **64**, 1815 (2001).
[3] V. Risberg, Arch. Math. Naturvidenskab **53**, 1 (1956).
[4] I. C. Percival, Proc. Phys. Soc. London, Sect. A **70**, 494 (1957).
[5] J. Shumway and D. M. Ceperley, Phys. Rev. B **63**, 165209 (2001).
[6] S. Chiesa, M. Mella, and G. Morosi, Phys. Rev. A **66**, 042502 (2002).
[7] M. van Faassen, A. Wasserman, E. Engel, F. Zhang, and K. Burke, Phys. Rev. Lett. **99**, 043005 (2007).
[8] K. M. Nollett, S. C. Pieper, R. B. Wiringa, J. Carlson, and G. M. Hale, Phys. Rev. Lett. **99**, 022502 (2007).
[9] G. F. Gribakin and J. Ludlow, Phys. Rev. A **70**, 032720 (2004).
[10] Y. Cheng, L. Y. Tang, J. Mitroy, and M. S. Safronova, Phys. Rev. A **89**, 012701 (2014).
[11] W. R. Johnson, S. A. Blundell, and J. Sapirstein, Phys. Rev. A **37**, 307 (1988).
[12] Y.-B. Tang, B.-Q. Lou, and T.-Y. Shi, Phys. Rev. A **96**, 022513 (2017).
[13] Y.-B. Tang, N.-N. Gao, B.-Q. Lou, and T.-Y. Shi, Phys. Rev. A **98**, 062511 (2018).
[14] M. Kurokawa, M. Kitajima, K. Toyoshima, T. Kishino, T. Odagiri, H. Kato, M. Hoshino, H. Tanaka, and K. Ito, Phys. Rev. A **84**, 062717 (2011).
[15] A. Chodos, R. L. Jaffe, K. Johnson, C. B. Thorn, and V. F. Weisskopf, Phys. Rev. D **9**, 3471 (1974).
[16] M. E. Rose, *Relativistic Electron Theory* (Wiley, New York, 1961).
[17] J. Mitroy, M. S. Safronova, and C. W. Clark, J. Phys. B **43**, 202001 (2010).
[18] T. F. O'Malley, L. Rosenberg, and L. Spruch, Phys. Rev. **125**, 1300 (1962).
[19] T. F. O'Malley, Phys. Rev. **130**, 1020 (1963).
[20] S. J. Buckman and J. Mitroy, J. Phys. B **22**, 1365 (1989).
[21] B. Mielewska, I. Linert, G. C. King, and M. Zubek, Phys. Rev. A **69**, 062716 (2004).
[22] J. C. Gibson, R. J. Gulley, J. P. Sullivan, S. J. Buckman, V. Chan, and P. D. Burrow, J. Phys. B **29**, 3177 (1996).
[23] C. Szmytkowski, K. Maciag, and G. Karwasz, Phys. Scr. **54**, 271 (1996).
[24] J. E. Furst, D. E. Golden, M. Mahgerefteh, J. Zhou, and D. Mueller, Phys. Rev. A **40**, 5592 (1989).
[25] M. Weyhreter, B. Barzick, A. Mann, and F. Linder, Z. Phys. D **7**, 333 (1988).
[26] K. P. Subramanian and V. Kumar, J. Phys. B **20**, 5505 (1987).
[27] S. J. Buckman and B. Lohmann, J. Phys. B **19**, 2547 (1986).
[28] J. Ferch and W. Raith, J. Phys. B **18**, 967 (1985).
[29] S. K. Srivastava, H. Tanaka, A. Chutjian, and S. Trajmar, Phys. Rev. A **23**, 2156 (1981).
[30] J. F. Williams, J. Phys. B **12**, 265 (1979).
[31] B. Schmidt, K. Berkhan, B. Götz, and M. Müller, Phys. Scr. **T53**, 30 (1994).
[32] M. Suzuki, T. Taniguchi, and H. Tagashira, J. Phys. D **23**, 842 (1990).
[33] Y. Nakamura and M. Kurachi, J. Phys. D **21**, 718 (1988).
[34] G. N. Haddad and T. F. O'Malley, Aust. J. Phys. **35**, 35 (1982).
[35] H. B. Milloy, R. W. Crompton, J. A. Rees, and A. G. Robertson, Aust. J. Phys. **30**, 61 (1977).
[36] R. P. McEachran and A. D. Stauffer, J. Phys. B **16**, 4023 (1983).
[37] R. P. McEachran and A. D. Stauffer, Aust. J. Phys. **50**, 511 (1997).
[38] R. P. McEachran and A. D. Stauffer, Eur. Phys. J. D **68**, 153 (2014).
[39] D. J. R. Mimnagh, R. P. McEachran, and A. D. Stauffer, J. Phys. B **26**, 1727 (1993).
[40] H. P. Saha, Phys. Rev. A **43**, 4712 (1991).
[41] H. P. Saha, Phys. Rev. A **47**, 273 (1993).
[42] O. Zatsarinny, Y. Wang, and K. Bartschat, Phys. Rev. A **89**, 022706 (2014).
[43] J. E. Sienkiewicz and W. E. Baylis, J. Phys. B **20**, 5145 (1987).
[44] S. N. Nahar and J. M. Wadehra, Phys. Rev. A **35**, 2051 (1987).
[45] J. E. Bloor and R. E. Sherrod, J. Phys. Chem. **90**, 5508 (1986).
[46] A. Dasgupta and A. K. Bhatia, Phys. Rev. A **32**, 3335 (1985).
[47] K. L. Bell, N. S. Scott, and M. A. Lennon, J. Phys. B **17**, 4757 (1984).
[48] W. C. Fon, K. A. Berrington, P. G. Burke, and A. Hibbert, J. Phys. B **16**, 307 (1983).
[49] BSR database, www.lxcat.net, retrieved on June 21, 2020.
[50] M. Adibzadeh and C. E. Theodosiou, At. Data Nucl. Data Tables **91**, 8 (2005).
[51] M. M. Haque, A. K. F. Haque, D. H. Jakubassa-Amundsen, M. A. R. Patoary, A. K. Basak, M. Maaza, B. C. Saha, and M. A. Uddin, J. Phys. Commun. **3**, 045011 (2019).
[52] Z. L. Petrovic, T. F. O'Malley, and R. W. Crompton, J. Phys. B **28**, 3309 (1995).
[53] V. J. Zigman and B. S. Milic, J. Phys. B **21**, 2609 (1988).
[54] G. J. Boyle, M. J. E. Casey, R. D. White, Y. Cheng, and J. Mitroy, J. Phys. D **47**, 345203 (2014).
[55] R. Panajotovic, D. Filipovic, B. Marinkovic, V. Pejcev, M. Kurepa, and L. Vuskovic, J. Phys. B **30**, 5877 (1997).
[56] R. P. McEachran and A. D. Stauffer, Eur. Phys. J. D **69**, 106 (2015).
[57] G. Hanel, B. Gstir, S. Denifl, P. Scheier, M. Probst, B. Farizon, M. Farizon, E. Illenberger, and T. D. Märk, Phys. Rev. Lett. **90**, 188104 (2003).